6. R. F. Service, *Science* **278**, 33 (1997).
7. E. J. Beckman, *Science* **283**, 946 (1999).
8. S. B. Roscoe, J. M. J. Fréchet, J. F. Walzer, A. J. Dias, *Science* **280**, 270 (1998).
9. G. W. Coates and R. M. Waymouth, *Science* **267**, 217 (1995).
10. T. R. Younkin *et al.*, *Science* **287**, 460 (2000).
11. F. C. Stehling, U.S. Patent 5,008,204 (1991).
12. J. C. Stevens, U.S. Patent 5,064,802 (1991).
13. H.-H. Shih, C.-M. Wong, Y.-C. Wang, C.-J. Huang, C.-C. Wu, *J. Appl. Polym. Sci.* **73**, 1769 (1999).
14. J. C. Whittmann and B. Lotz, *Prog. Polym. Sci.* **15**, 909 (1990).
15. G. M. Brown and J. H. Butler, *Polymer* **38**, 3937 (1997).
16. The noncrystallizable portion of the zPE polymer was determined to be relatively low molecular mass ($M_w \approx$ 30,000 daltons) and highly branched material (more than 14% branched repeat units) as determined by temperature rising elution fractionation (TREF) [L. Wild, T. R. Ryle, D. C. Knobeloch, I. R. Peat, *J. Polym. Sci. Polym. Phys. Ed.* **20**, 441 (1982)] and gel permeation chromatography (GPC).
17. D. Broseta, G. H. Fredrickson, E. Helfand, L. Leibler, *Macromolecules* **23**, 132 (1990).
18. S. H. Anastasiadis, I. Gancar, J. T. Koberstein, *Macromolecules* **21**, 2980 (1988).
19. D. C. Bassett, *Principles of Polymer Morphology* (Cambridge Univ. Press, New York, 1981).
20. E. Helfand and A. Sapse, *J. Chem. Phys.* **62**, 1327 (1975).
21. K. A. Chaffin, F. S. Bates, G. M. Brown, P. Brant, *J. Polym. Sci. Polym. Phys.* **38**, 108 (2000).
22. Linear dynamic mechanical spectroscopy measurements indicate that all PE and *i*PP polymer chain relaxation times are less than 0.1 s at the laminate molding temperature. Hence, the 10-min molding time far exceeds the time required to achieve an equilibrium interfacial composition profile.
23. C. Creton, E. J. Kramer, G. Hadziioannou, *Macromolecules* **24**, 1846 (1991).
24. H. R. Brown, *Macromolecules* **22**, 2859 (1989).
25. _____, V. R. Deline, P. F. Green, *Nature* **341**, 221 (1989).
26. L. J. Fetters, D. J. Lohse, D. Richter, T. A. Witten, A. Zirkel, *Macromolecules* **27**, 4639 (1994).
27. Y. H. Kim and R. P. Wool, *Macromolecules* **16**, 1115 (1983).
28. D. Adolf, M. Tirrell, S. Prager, *J. Polym. Sci. Polym. Phys.* **23**, 413 (1985).
29. H. H. Krausch and M. Tirrell, *Annu. Rev. Mater. Sci.* **26**, 651 (1989).
30. Because molecular conformations are perturbed by crystallization, PE/*i*PP weld strength may be affected by laminate cooling rate, as shown by Lin *et al.* (*32*). Experiments with mPE/m*i*PP laminates confirm that peel strength decreases with decreasing cooling rate. This is not a consequential factor with glassy polymers because vitrification is essentially uncorrelated with chain conformation.
31. Peel tests on laminated films of Ziegler-Natta *i*PP and ethylene-propylene (block) copolymer (*32*) resulted in adhesive strengths comparable to those reported here for the Ziegler-Natta polymers, that is, more than an order of magnitude lower than the failure strength of the all-metallocene materials.
32. G. Lin, W. Wenig, J. Petermann, *Angew. Makromol. Chem.* **255**, 33 (1998).

33. Financial support was provided to the University of Minnesota by the Exxon Chemical Company. TEM and x-ray scattering measurements were conducted at the University of Minnesota Materials Research Science and Engineering Center–supported Institute of Technology Characterization Facility.

20 March 2000; accepted 4 May 2000

Understanding the Distribution of Near-Earth Asteroids

William F. Bottke Jr.,[1] Robert Jedicke,[2] Alessandro Morbidelli,[3] Jean-Marc Petit,[3] Brett Gladman[3]

We have deduced the orbital and size distributions of the near-Earth asteroids (NEAs) by (i) numerically integrating NEAs from their source regions to their observed orbits, (ii) estimating the observational biases and size distribution associated with asteroids on those orbits, and (iii) creating a model population that can be fit to the known NEAs. We predict that there are ~900 NEAs with absolute magnitude less than 18 (that is, kilometer-sized), of which 29, 65, and 6% reside on Amor, Apollo, and Aten orbits, respectively. These results suggest that roughly 40% of the kilometer-sized NEAs have been found. The remainder, on highly eccentric and inclined orbits, are more difficult to detect.

Most NEAs [definition in (*1*)] are believed to be fragments of main belt asteroids that, after ejection in a collision event involving a larger asteroid millions of years ago, wandered through space until reaching an Earth-approaching orbit (*2*). Evidence from the lunar and terrestrial crater record indicates that this population has bombarded Earth over the age of the solar system, and related geologic evidence indicates that the collision of a multi-kilometer asteroid with Earth can wreak regional-to-global devastation on our biosphere (*3*).

Despite widespread recognition of the NEA impact hazard (*4*), the distributions of NEA orbits and sizes remain uncertain. As of April 2000, ~950 NEAs have been detected that have absolute magnitude H between 10 and 29 (*5*), roughly corresponding to asteroid diameters D between 40 and 0.01 km (*6*). It is likely that only NEAs brighter than $H \sim 14$ ($D > 7$ km) have been completely discovered (*7, 8*); these 16 objects are too few to help determine the orbital distribution of the smaller NEAs. An added complication is that the observed distribution of $H > 14$ NEAs is heavily skewed because (i) they were discovered piecemeal by different asteroid survey programs following a variety of detection strategies; and (ii) each survey is flux-limited, so that the volume of space it investigates varies strongly with H (*9*, *10*). Even worse, our understanding of the orbital paths taken by bodies to replenish the NEA population is incomplete, making it difficult to use specific NEAs as tracers of large-scale dynamical processes. Interpreting the orbital distribution of the NEA population, therefore, requires a knowledge of the detection biases involved and a characterization of the statistical evolution of NEAs from their sources.

To attack these problems, we constructed a steady-state model of the orbital and size distributions of the NEAs (*11*). NEA orbits were generated by tracking the dynamical evolution of test bodies coming out of three so-called intermediate sources (ISs): regions that are constantly fed material escaping the main belt. The relative contributions of the ISs are expressed through weighting coefficients. The NEA size distribution, assumed to be orbit-independent, was constructed so that its shape could be manipulated using a single parameter. Combining these components with the observational biases associated with the Spacewatch NEA survey, we obtained a model distribution (with three adjustable parameters) that could be fit to the orbits and sizes of the NEAs discovered or accidentally rediscovered by Spacewatch. The best-fit parameters extracted from this technique were then used to calculate the debiased NEA population.

The physical and orbital properties of NEAs suggest that many originated in the main belt (*2*). Asteroid fragments, liberated during collisions in the main belt, are directly injected (*12*) or slowly moved via Yarkovsky thermal drag (*13*) into both mean-motion resonances with the planets and so-called secular resonances, where orbital frequencies are commensurate with the solar system's natural frequencies (*14*). These mechanisms create three important ISs for the NEAs: (i) asteroids in the 3:1 mean-motion resonance with Jupiter; (ii) asteroids in the ν_6 secular resonance; and (iii) asteroids on Mars-crossing orbits adjacent to the main belt, which have not yet entered the NEA region. The eccentricities (and inclinations) of the IS asteroids are modified by resonant perturbations and/or planetary encounters until they reach the NEA region (*15–17*). Other potential IS regions (for example, asteroids in the 5:2 resonance with Jupiter) provide relatively few NEAs (*18*).

To understand the orbital paths followed

[1]Center for Radiophysics and Space Research, Cornell University, Ithaca, NY 14853–6801, USA. [2]Lunar and Planetary Laboratory, University of Arizona, Tucson, AZ 85721, USA. [3]Observatoire de la Côte d'Azur, Boite Postale 4229, 06034 Nice Cedex 4, France.

To whom correspondence should be addressed. E-mail: bottke@astrosun.tn.cornell.edu

by NEAs from our IS regions, we start test bodies in each IS and track them as they cross a network of semimajor axis, eccentricity, inclination (a, e, i) cells placed in the NEA region. Each (a, e, i) cell is 0.06 astronomical units (AU) × 0.02 × 5° in volume. The test bodies were followed with the use of the mixed-variable symplectic N-body code swift-rmvs3 (*19*). Gravitational perturbations from the planets Venus through Neptune were included in our integrations. Test bodies entering the NEA region were followed until they collided with the sun or a planet or were thrown beyond 10 AU, usually by a close encounter with Jupiter. We call these end states the sinks. Few objects (<1%) entering the NEA region were found to live longer than 100 million years (My), the nominal length of our integrations. Those that did were tracked until they were removed by a sink. Rare end states, such as collisional or tidal disruption events, were not included (*20*).

To determine the steady-state orbital distribution of NEAs coming from each IS, we calculated the cumulative time that particles spent in each cell and normalized those values by the total time spent in all cells. The resultant residence time probability distribution $R_{IS}(a, e, i)$ shows where asteroids from each IS statistically spend their time in the NEA region (*21*). To prevent under- or overestimates in R_{IS}, the initial orbits of the test bodies were placed outside the NEA region.

$R_{3:1}(a, e, i)$ was calculated by tracking 2354 test bodies ($e < 0.35$; $i < 15°$) started within the boundaries of the 3:1 mean-motion resonance with Jupiter, located at ~2.5 AU (*16*, *21*) (Fig. 1). Strong resonant e pumping allowed most bodies to reach NEA orbits in ~1 My. Tests indicated that starting conditions have little influence on test body outcomes. The average time spent by a test body in the NEA region before entering a sink was 2.2 My. Only 38% of the steady-state NEA population coming from the 3:1 resonance had $a < 2$ AU: the region where most known NEAs reside.

For $R_{\nu 6}(a, e, i)$, we followed 3519 test bodies started in the strong portion of the ν_6 secular resonance (*22*), where periodic oscillations in e caused by the resonance can move them onto NEA orbits in ~1 My (*16, 21*) (Fig. 1). The average time spent by these objects in the NEA region was 6.5 My. Seventy percent of the steady-state population coming from the ν_6 resonance attained $a < 2$ AU, nearly twice the fraction of the 3:1 NEAs.

Our third IS is the component of the Mars-crossing asteroid population adjacent to the main belt. Bodies in this region, defined as intermediate source Mars-crossers (IMCs), have orbital parameters $q > 1.3$ AU, 2.06 AU $\leq a \leq$ 2.48 AU, or 2.52 AU $\leq a <$ 2.8 AU, i below the location of the ν_6 resonance [$i \sim$ 15° or less (*21*)] and a combination of (a, e, i) values such that they cross the orbit of Mars during a secular oscillation cycle of their eccentricity (*17*). To offset leakage into the NEA region, these IMC objects are resupplied predominantly by numerous Mars- and three-body (such as Jupiter-Saturn-asteroid) mean-motion resonances (*17*) and by material in the vicinity of the ν_6 resonance (*23*). Our numerical simulations suggest that the IMCs are a primary source of NEAs; other populations on Mars-crossing orbits are not as effective, with the exception of those bodies that are members of the other two ISs described in this paper.

The IMC population changes over time as secular perturbations modify Mars's eccentricity. To ensure that past, present, and future IMC asteroids were accounted for, we integrated 2977 known asteroids with perihelia 1.3 AU < $q <$ 1.8 AU, 2.00 AU < $a <$ 2.8 AU, and $i <$ 15° (*5*). Asteroids started near the 3:1 resonance or well inside the ν_6 resonance were removed from our outcome statistics (*21*). We found that 755 of these bodies entered the NEA region over the integration time. These bodies were tracked until they entered one of the sinks, and their orbital paths were used to generate $R_{IMC}(a, e, i)$. To make sure that $R_{IMC}(a, e, i)$ was not dependent on initial conditions, we independently integrated a smaller set of objects with 1.3 AU < $q <$ 1.78 AU. Although fewer objects (542) entered the NEA region, no significant differences were seen in the shape of $R_{IMC}(a, e, i)$. For this reason, our final version of $R_{IMC}(a, e, i)$ includes data from both sets. A complication in using real IMC asteroids to map orbital paths in the NEA region is that these objects are biased by observational selection. To compensate for this effect, we weighted the orbital paths of all IMCs with a numerical factor corresponding to the observational biases associated with their starting orbit (*23*).

The results for $R_{IMC}(a, e, i)$ (Fig. 1) suggest that the mechanisms pushing IMCs onto Earth-crossing orbits are weak, so that many objects evolve along the $q \sim 1$ AU line by Earth encounters (*24*). The average time spent by an IMC object in the NEA region before entering a sink was 3.85 My. In this case, 53% of the steady-state NEA population from the IMC region had $a < 2$ AU.

Each $R_{IS}(a, e, i)$ described above produces a characteristic orbital distribution that is different from the others. This property allows us to model the steady-state orbital distribution of the NEAs [$R_{NEA}(a, e, i)$] as a linear combination of $R_{IS}(a, e, i)$ multiplied by unknown weighting factors (α_{IS})

$$R_{NEA} = \alpha_{3:1}R_{3:1} + \alpha_{\nu 6}R_{\nu 6} + \alpha_{IMC}R_{IMC} \quad (1)$$

The sum of all α_{IS} values is 1.0, with $0.0 \leq \alpha_{IS} \leq 1.0$.

Now that we have a function describing the NEA orbital distribution, we can examine the NEA absolute magnitude distribution $N_{NEA}(H)$. We assume that each IS has the same size distribution. We concentrate on the $13 < H < 22$ range (*26*). The shape of $N_{NEA}(H)$ was determined by testing several functional forms with free parameters. Some of our trial assumptions were based on previous work (*10*, *27*, *28*). Our most successful characterization of the differential distribution $N_{NEA}(H)$ for $13 < H < 22$ was

$$N_{NEA}(H) = C \times 10^{\gamma(H-13)} \quad (2)$$

where γ is a free parameter and C is a constant set by the total number of NEAs with $13 < H < 15$.

Our model of the debiased orbital and size

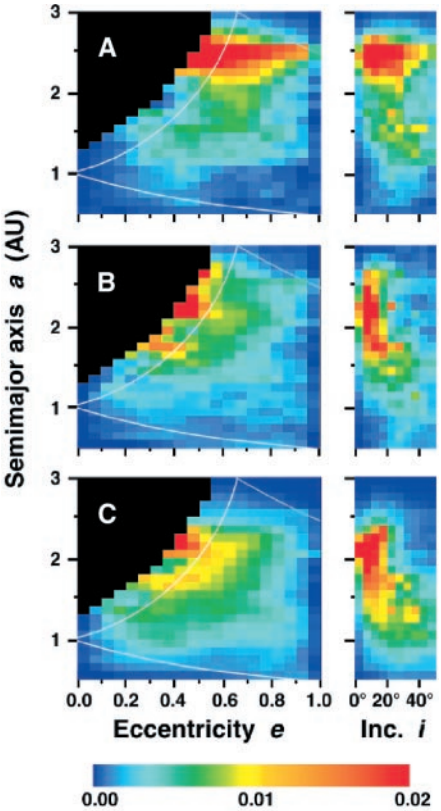

Fig. 1. A representation of the probability distributions of residence time [$R_{IS}(a, e, i)$] for NEAs evolving out of our three ISs: (**A**) 3:1 mean-motion resonance with Jupiter, (**B**) the IMC region, and (**C**) ν_6 secular resonance. The sum of the (a, e, i) bins in the NEA target region (0.5 AU < $a <$ 2.8 AU; $e < 0.8$, $i < 35°$) has been normalized to 1.0. To display as much of the (a, e, i) distribution as possible in two dimensions, we summed the i bins before plotting $R_{IS}(a,e)$, whereas the e bins were summed before plotting $R_{IS}(a,i)$. The color scale depicts the expected density of NEAs in a scenario of steady-state replenishment from the IS regions. Red colors indicate where NEAs are statistically most likely to spend their time. Bins whose centers have perihelia $q > 1.3$ AU are not used and are colored black. The white curved lines represent the values needed for an Earth-crossing orbit. The gray curve in the upper right indicates where objects cross the orbit of Jupiter.

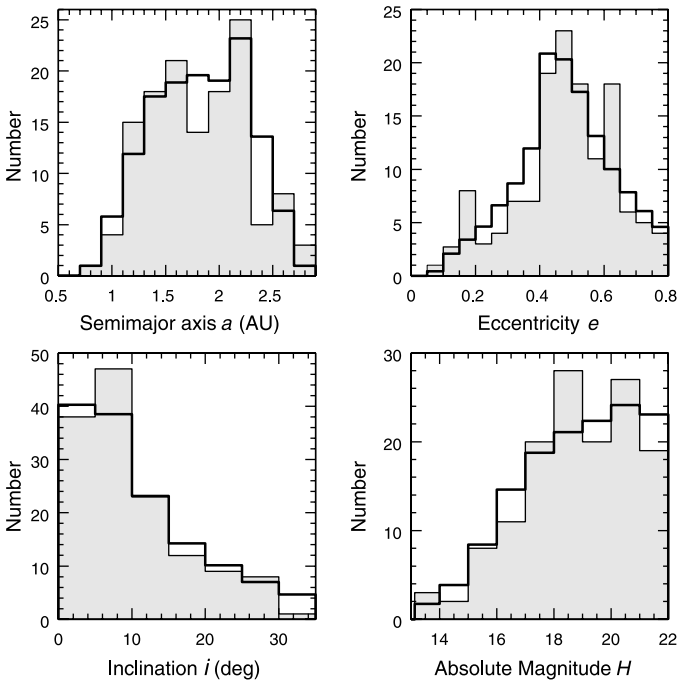

Fig. 2. A comparison between the 138 Spacewatch NEAs (shaded histogram) and $n(a, e, i, H)$ (dark solid line), our best fit of the observed NEA probability distribution assuming $\alpha_{3:1}$, α_{MC}, $\alpha_{\nu 6}$ = 0.36, 0.29, 0.35, respectively, and $\gamma = 0.35$. The parameters are linked to the NEA target region (0.5 AU $< a <$ 2.8 AU; $e <$ 0.8, $i < 35°$; $H < 22$). Our four-dimensional (a, e, i, H) distribution has been collapsed into one dimension for this comparison.

distribution of the NEAs, $M(a, e, i, H)$, is

$$M(a, e, i, H) = R_{\mathrm{NEA}}(a, e, i) \times N_{\mathrm{NEA}}(H) \quad (3)$$

If the free parameters α_{IS} and γ reflect actual NEA values, we can use our model to describe the orbital and size distributions of all NEAs with $H < 22$ (that is, larger than ~170 m in diameter).

To determine α_{IS} and γ, we need to compare M with the known NEAs. This cannot be done until we compensate for NEA discovery biases. Because each asteroid survey finds objects based on its search strategy, the limiting magnitude of its detector, and its system characteristics, each survey has unique discovery biases. For this reason, we focus here on debiasing results from the Spacewatch NEA search program, whose observing methodology and apparatus are well documented (*9*, *10*).

We used an earlier calculation of the bias $B(a, e, i, H)$ (*10*) for the Spacewatch detector system. The bias is a correction factor ($n = BN$) between the observed number (n) and actual number (N) of asteroids in an (a, e, i, H) bin per square degree at opposition at the vernal equinox. It can be thought of as an asteroid detection probability. Here, B has been calculated for the range 0.5 AU $< a <$ 2.8 AU, $e < 0.8$, $i <$ 35°, and $H < 22$, which we define as the NEA target region. High B values correspond to easily detected asteroids, whereas low B values correspond to difficult-to-detect asteroids (*29*).

Only a small proportion of Spacewatch's detections are NEAs. To separate NEAs from more numerous background asteroids, Spacewatch calculates the angular rate of motion for each detected body and uses this value as a discriminant. At opposition, objects with ecliptic latitude rates between ±0.3 degrees per day and ecliptic longitude rates between −0.2 to −0.3 degrees per day are usually main belt or IMC asteroids (*10*). Asteroids with rates of motion outside this zone are flagged as potential NEAs and are followed over several observing nights until an orbit solution is obtained. If that solution yields $q < 1.3$ AU, Spacewatch reports an NEA discovery. This method, although useful, eliminates some NEAs; perhaps a third of all of Spacewatch's NEA detections have rates of motion that mimic typical main belt asteroids. Most excluded NEAs have $a > 2$ AU. The bias calculation we use incorporates a filter based on Spacewatch's selection of NEAs in the determination of the correction factor B. We call this more specific bias B_{NEA} (*30*).

Using B_{NEA}, our predicted distribution for the observed Spacewatch NEAs is

$$n(a,e,i,H) = B_{\mathrm{NEA}}(a,e,i,H) \times M(a,e,i,H) = B_{\mathrm{NEA}}(a,e,i,H)\, R_{\mathrm{NEA}}(a,e,i)\, N_{\mathrm{NEA}}(H) \quad (4)$$

To simultaneously test in four dimensions how well this distribution matches real data, we compared n with 138 NEAs discovered and accidentally rediscovered by Spacewatch (*31*), using a maximum-likelihood technique (*32*). We computed the best-fit parameters α_{IS} and γ by maximizing the likelihood value. Our best fit yielded $\alpha_{3:1} = 0.36^{+0.19}_{-0.14}$ and $\alpha_{\mathrm{IMC}} = 0.29^{+0.13}_{-0.20}$, with $\alpha_{\nu 6}$ constrained by the relation $\alpha_{3:1} + \alpha_{\mathrm{IMC}} + \alpha_{\nu 6} = 1.0$. At the best-fit values, $\alpha_{\nu 6} = 0.35$. The best-fit $\gamma = 0.35 \pm 0.02$. The statistical errors of our fit were determined with a Monte Carlo method (*33*). These values only apply to the specified NEA target region. The parameter C in Eq. 2 is then fixed by imposing that $\int_{13}^{15} N_{\mathrm{NEA}}(H)dH = 66$ (*34*). With the best-fit value of γ reported above, we obtain $C = 13.26$.

We can graphically compare our 138 Spacewatch NEAs to our best-fit case by collapsing our results into four one-dimensional plots over a, e, i, H (Fig. 2). We find that our three IS regions account for the vast majority of known NEAs, so that our estimate for $M(a, e, i, H)$ should be accurate enough for general use by observers and theoreticians. The quality of the fit also implies that additional sources of NEAs, such as extinct comets (*35*), cannot produce a significant fraction of $H < 22$ NEAs unless they also produce orbital signatures similar to those of R_{IS} regions already considered.

Using the best-fit parameters for the NEA target region, we derive $M(a, e, i, H)$, the debiased orbital and size distributions for the entire NEA region ($e < 1.0$, $i < 90°$, $H <$ 22). The contributions of the IS regions (3:1, IMC, and ν_6) to M are 40, 27, and 33%, respectively. These values deviate from α_{IS} because the 3:1 resonance pumps up asteroid e and i values beyond the limits of the target region, which in turn increases its contribution to the NEA population at the expense of the other IS regions.

The results for the debiased population (Fig. 3) focus on $H < 18$ objects alone because these bodies, roughly ~ 1 km in diameter (*6*), are thought to produce global destruction when striking Earth (*4, 27*) (Table 1). Starting with the NEA H distribution, we find that our estimate of the power law exponent $\gamma = 0.35 \pm 0.02$ for $N_{\mathrm{NEA}}(15 < H <$ 22) is the same as that derived by earlier analyses of Spacewatch data (*36*) and by the NEAT asteroid survey using debiased data (*8*). We predict that there are $\sim 910^{+100}_{-120}$ NEAs with $H < 18$, which is about a factor of 1.5 to 2.0 lower than pre-1999 estimates (*27*, *28*), but 1.3 times larger than that of Rabinowitz *et al.* (*8*), who used a different normalization method.

About half of the NEA population has $a \geq 2$ AU. Objects in this region are generally removed within a few million years by solar collisions or through close encounters with Jupiter. The remaining NEAs reach $a < 2$ AU orbits by encounters with the terrestrial planets, though they must first survive passage through multiple resonances between 1.8 and 2.0 AU (that is, 4:1 and 5:1 mean-motion resonance with Jupiter; ν_6 and ν_{16} secular resonances). In terms of observational completeness, we

predict that ~40% of the $H < 18$ (kilometer-sized) NEAs have been discovered. Many NEAs with $e \leq 0.4$ and $i \leq 10°$ have been discovered (~70 and ~60%, respectively). These NEAs are relatively easy targets for asteroid surveys. A significant number of NEAs, however, hide at high a, e, and i values, making them more difficult to detect.

The fractions of NEAs with $15 < H < 22$ on Amor, Apollo, and Aten orbits (*1*) are 29 ± 2%, 65 ± 2%, and 6 ± 2%, respectively. Few Atens exist because the orbital pathways to this region are long and tortuous enough that significant attrition occurs. Using our best-fit parameters, we predict there are 260^{+40}_{-60} Amors, 590^{+90}_{-100} Apollos, and 56^{+11}_{-33} Atens with $H < 18$. These values suggest that ~30% of the km-sized Apollos and Atens and nearly 70% of the Amors have been discovered. Amors generally have higher B_{NEA} and lower e, i than do Apollos and Atens, which may explain this disparity. The asteroid population residing inside Earth's orbit (aphelia $Q < 0.983$ AU) is about 2% of the NEA population. We predict that there are 20^{+4}_{-6} of the bodies with $H < 18$, with nearly all residing on Venus-crossing orbits.

We can also infer how much material comes from the various IS regions. About 43% of the Apollos and 36% of the Amors come from the 3:1 resonance. In terms of orbitally evolved populations (those closest to the sun), 50% of the Atens and the $Q < 0.983$ AU asteroids come from the ν_6 resonance, probably because a large fraction of material from the ν_6 resonance (70%) reaches $a < 2$ AU.

Using the formula $D = 4365 \times 10^{-H/5}$ (*6*) with $\gamma = 0.35$ to transform $N_{NEA}(H)$ into a cumulative size distribution, we find that the average power law slope between 170-m and 4-km asteroids is ~1.8. This value is shallower than the slope for a population in simple collisional equilibrium [2.5 (*37*)] or one dominated by fresh collisional debris [>2.5 (*38*)], but it is reasonably close to the estimated size distribution of km-sized asteroids in the main belt (*10*). It also agrees with the size distributions of youthful cratered surfaces on Venus, Earth, Mars, and the moon (*39*).

If our derived slope is valid, it calls into question the scenario for NEA delivery that claims that main belt collisions resupply NEAs by directly injecting fragments into the 3:1 or ν_6 resonances (*12*). The mean lifetime of objects in the NEA region is only a few My—too short for collisions to significantly change the size distribution for fresh debris (*13*). It is possible that different IS regions have different size distributions, but it is unclear why collisional injection would work better in some main belt regions than in others.

Table 1. Statistics of steady-state NEA and aphelia $Q < 0.983$ AU populations. The definitions of the object classes are given in the text. The percentages refer to predicted values.

	NEA	Amor	Apollo	Aten	$Q < 0.983$ AU
No. of known NEAs with $H < 18$	356	172	165	19	0
No. of predicted NEAs with $H < 18$	910	260	590	56	20
Observed completeness for $H < 18$ NEAs (%)	39	66	28	34	0
$a < 2.0$ AU (%)	52	31	57	100	100
$e < 0.4$ (%)	16	29	9	29	45
$e < 0.6$ (%)	55	98	36	55	69
$i < 10°$ (%)	22	37	16	5	8
$i < 20°$ (%)	48	67	43	19	26
$i < 30°$ (%)	67	83	62	42	48

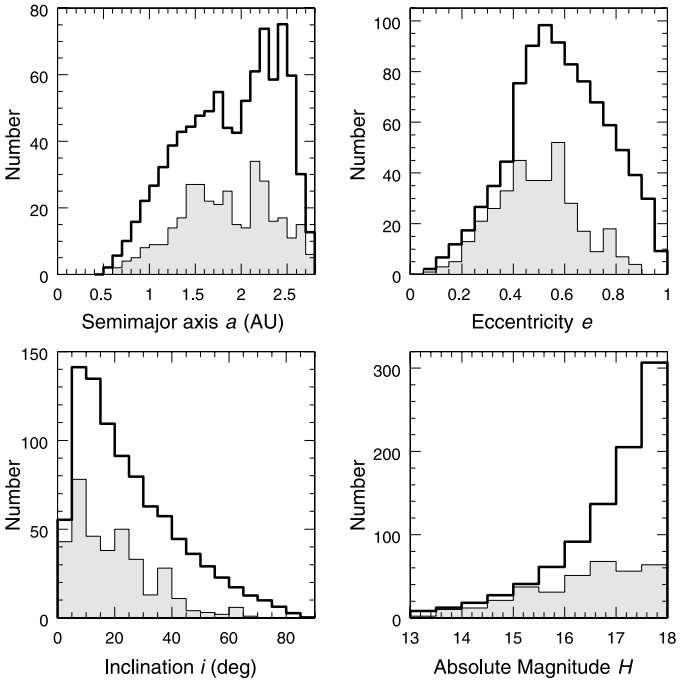

Fig. 3. The debiased orbital and size distribution of the NEAs for $H < 18$. The predicted NEA distribution (dark solid line) is normalized to 910 NEAs. It is compared with the 356 known NEAs from all surveys (shaded histogram). Current NEA observational completeness is ~40%, with a preponderance of objects discovered at low e and i.

An alternative NEA delivery scenario, which is more consistent with our model results, is that main belt asteroids drift into the 3:1 or ν_6 resonances via some drag force such as the Yarkovsky effect (*13*). The expected drift for km-sized bodies is ~ ± 10^{-4} AU My^{-1}: slow enough for new debris to undergo collisional evolution before entering the IS. The NEA and IS size distributions, therefore, may be extensions of the main belt size distribution between 2.1 and 2.8 AU.

If the Yarkovsky effect is the dominant means by which asteroids enter the IS, we expect α_{IS} to vary with size. Numerical simulations show that small objects, with fast drift rates, jump over the tiny resonances feeding the MC regions to enter the powerful 3:1 or ν_6 resonances (*13*). Conversely, the largest NEAs (such as 433 Eros) are hardly affected by the Yarkovsky effect, so that their most likely source would be the numerous tiny resonances feeding the IMC region (*17*). In terms of our model results, the α_{IS} values we find may be more characteristic of km and sub-km NEAs than of multi-kilometer NEAs because two-thirds of the Spacewatch NEAs have $18 < H < 22$.

References and Notes

1. NEAs have perihelion distances $q \leq 1.3$ AU and aphelion distances $Q \geq 0.983$ AU. NEA subgroups include the Amors (1.0167 AU $< q \leq 1.3$ AU); Apollos ($a \geq 1.0$ AU, $q \leq 1.0167$ AU), and Atens ($a < 1.0$ AU, $Q \geq 0.983$ AU). D. Rabinowitz, E. Bowell, E. M. Shoemaker, K. Muinonen, in *Hazards due to Comets and Asteroids*, T. Gehrels, Ed. (Univ. of Arizona Press, Tucson, AZ, 1994), pp. 285–312.
2. L. A. McFadden, D. J. Tholen, G. J. Veeder, in *Asteroids II*, R. P. Binzel, T. Gehrels, M. S. Matthews, Eds. (Univ. of Arizona Press, Tucson, AZ, 1989), pp. 442–467.
3. See, for instance, the chapters by G. Neukum and B. A. Ivanov; O. B. Toon, K. Zahnle, R. P. Turco, and C. Covey; and M. R. Rampino and B. M. Haggerty, in *Hazards due to Comets and Asteroids*, T. Gehrels, Ed. (Univ. of Arizona Press, Tucson, AZ, 1994), pp. 359–416, pp. 791–826, and pp. 827–858, respectively.
4. C. R. Chapman and D. Morrison, *Nature* **367**, 33 (1994).
5. We used the April 2000 update of the public-domain asteroid orbit database "astorb.dat" found at http://asteroid.lowell.edu. See also E. Bowell, K. Muinonen, and L. H. Wasserman, in *Asteroids, Comets, Meteors 1993*, A. Milani, M. DiMartino, A. Cellino, Eds. (Kluwer, Dordrecht, Netherlands, 1994), pp. 477–481.
6. Transforming H into a characteristic NEA diameter

is problematic. We use a bolometric geometric albedo that favors S-type asteroids ($p \sim 0.155$). See D. J. Tholen and M. A. Barucci [in *Asteroids II*, R. P. Binzel, T. Gehrels, M. S. Matthews, Eds. (Univ. of Arizona Press, Tucson, AZ, 1989), pp. 298–315] for details. We convert between absolute magnitude H and diameter D using $D = 4365 \times 10^{-H/5}$ [E. Bowell *et al*., in *Asteroids II*, R. P. Binzel, T. Gehrels, M. S. Matthews, Eds. (Univ. of Arizona Press, Tucson, AZ, 1989), pp. 524–556].

7. E. M. Shoemaker, R. F. Wolfe, C. S. Shoemaker, in *Global Catastrophes in Earth History*, V. L. Sharpton and P. D. Ward, Eds. (Geological Society of America Special Paper 247); A. W. Harris, in *Collisional Processes in the Solar System*, M. Marov and H. Rickman, Eds. (Kluwer, in press).
8. D. L. Rabinowitz, E. Helin, K. Lawrence, S. Pravdo, *Nature* **403**, 165 (2000).
9. D. L. Rabinowitz, *Icarus* **111**, 364 (1994).
10. R. Jedicke, *Astron. J.* **111**, 970 (1996); R. Jedicke and T. S. Metcalfe, *Icarus* **131**, 245 (1998); D. D. Durda, R. Greenberg, R. Jedicke, *Icarus* **135**, 431 (1998).
11. tk;4Studies suggest that the cratering flux on the Earth-moon system has been more or less constant for the past ~3 billion years. If true, the NEA population has been in a steady state over that same time [R. A. F. Grieve and E. M. Shoemaker, in *Hazards due to Comets and Asteroids*, T. Gehrels, Ed. (Univ. of Arizona Press, Tucson, AZ, 1994), pp. 417–462].
12. P. Farinella, R. Gonczi, Ch. Froeschlé, Cl. Froeschlé, *Icarus* **101**, 174 (1993).
13. P. Farinella, D. Vokrouhlický, W. K. Hartmann, *Icarus* **132**, 378 (1998); P. Farinella and D. Vokrouhlický, *Science* **283**, 1507 (1999); W. F. Bottke, D. P. Rubincam, J. A. Burns, *Icarus* **145**, 301 (2000).
14. J. G. Williams, *Eos* **54**, 233 (1973); J. Wisdom, *Icarus* **56**, 51 (1983).
15. P. Farinella *et al*., *Nature* **371** 314 (1994).
16. B. J. Gladman *et al*., *Science* **277**, 197 (1997).
17. F. Migliorini, P. Michel, A. Morbidelli, D. Nesvorný, V. Zappalà, *Science* **281**, 2022 (1998); A. Morbidelli and D. Nesvorný, *Icarus* **139**, 295 (1999); D. Nesvorný and A. Morbidelli, *Astron. J.* **116**, 3029 (1998); N. Murray, M. Holman, M. Potter, *Astron. J.* **116**, 2583 (1998); P. Michel, F. Milgiorini, A. Morbidelli, V. Zappala, *Icarus*, in press.
18. The ability of a resonance to produce NEAs is determined by its location, its efficiency at pushing objects onto high-e orbits, and the flux of asteroids entering the resonance over time. Powerful resonances beyond 2.8 AU (for example, the 5:2 resonance with Jupiter) frequently push objects directly onto Jupiter-crossing orbits, where they are ejected from the solar system in $\leq 10^5$ years. Few NEAs come from these transportation routes (*16*). Prominent resonances in the inner solar system, like the 3:1 mean-motion resonance with Jupiter and the ν_6 secular resonance, generally do not directly produce Jupiter-crossing objects. For this reason, these resonances have long been considered plausible wellsprings for meteorites and NEAs [G. W. Wetherill, *Meteoritics* **20**, 1 (1985); *Philos. Trans. R. Soc. London Ser. A* **323**, 323 (1987); *Icarus* **76**, 1 (1988)].
19. J. Wisdom and M. Holman, *Astron. J.* **102**, 1528 (1991); H. F. Levison and M. J. Duncan, *Icarus* **108**, 18 (1994).
20. A $H = 22$ NEA, with a diameter of about 170 m (*6*), has a collisional lifetime >100 My (*13, 16*). The mean lifetime of rubble-pile NEAs against tidal disruption with Earth or Venus is ~65 My [D. C. Richardson, W. F. Bottke, S. G. Lovek, *Icarus* **134**, 47 (1999); W. F. Bottke, D. C. Richardson, P. Michel, S. G. Love, *Astron. J.* **117**, 1921 (1999)]. Both time scales are longer than the NEA dynamical lifetimes reported here. We expect tidal disruption, however, to increase in importance as NEAs attain low e, i orbits.
21. A. Morbidelli and B. Gladman, *Meteorit. Planet. Sci.* **33**, 999 (1998); A. Morbidelli, *Icarus* **105**, 48 (1993).
22. Our numerical runs for the ν_6 resonance use test bodies started near each of the following positions: ($a \sim 2.06$ AU, $i = 2.5°$), ($a \sim 2.08$ AU, $i = 5°$), ($a \sim 2.115$ AU, $i = 7.5°$), ($a \sim 2.16$ AU, $i = 10°$), ($a \sim 2.24$ AU, $i = 12.5°$), and ($a \sim 2.315$ AU, $i = 15°$). For all cases, $e = 0.1$. Bodies clearly not on a fast track to NEA orbits were removed when calculating $R_{\nu 6}$. See (*21*) for details.
23. Not all IMC objects are produced via weak main belt resonances. Some bodies residing near (but not "in") the strong part of the ν_6 resonance have libration amplitudes large enough to reach Mars-crossing orbits [G. W. Wetherill and J. G. Williams, in *Origin and Distribution of the Elements*, L. H. Ahrens, Ed. (Pergamon, Oxford, 1979), pp. 19–31]. In addition, some current IMCs have been extracted from the 3:1 or ν_6 resonances via close encounters with Mars.
24. To interpret how the known MC asteroids are biased with respect to a and i, we divided the IMC and near-IMC regions ($q < 1.8$ AU) into three semimajor axis zones (zone a1: 2.1 AU $\leq a < 2.3$ AU; zone a2: 2.3 AU $\leq a < 2.5$ AU; zone a3: 2.5 AU $\leq a < 2.8$ AU) and three inclination zones (zone i1: $i < 5°$ AU; zone i2: $5° \leq i < 10°$; zone i3: $10° \leq i < 15°$) and estimated the observational biases for asteroids in those zones (*10*). The ratios of the biases in zones a2 and a3 over zone a1 were ~1.3 and ~1.8, respectively, whereas the ratios of the biases in zones i2 and i3 over zone i1 were ~2.7 and ~4.4, respectively. These values were used to weight the orbital paths of underrepresented IMCs in each zone when $R_{\mathrm{IMC}}(a, e, i)$ was calculated.
25. W. F. Bottke, M. C. Nolan, H. J. Melosh, A. M. Vickery, R Greenberg, *Icarus* **122**, 406 (1996).
26. We exclude Spacewatch NEAs with $H > 22$ because they are discovered by means of a different search strategy than are $H < 22$ objects (*9*).
27. D. Morrison, Ed., *The Spaceguard Survey: Report of the NASA International Near-Earth-Object Detection Workshop* (NASA, Washington, DC, 1992), pp. 1–19.
28. D. Rabinowitz, E. Bowell, E. M. Shoemaker, K. Muinonen, in *Hazards due to Comets and Asteroids*, T. Gehrels, Ed. (Univ. of Arizona Press, Tucson, AZ, 1994), pp. 285–312.
29. Objects with high B values correspond to bright/large objects and/or those that move slowly through Spacewatch's search volume (such as multi-km main belt asteroids, IMCs, and NEAs on low-i orbits with a between 2 and 3 AU). Conversely, low B values correspond to dim/small objects and/or those with such fast angular speeds that they spend little time in Spacewatch's search volume (such as sub-km NEAs that rarely approach Earth and high-i asteroids).
30. B_{NEA} can, in principle, be used to estimate the entire NEA population from the known NEAs without taking additional steps by dividing the observed population by the bias factor directly. This type of procedure has already been used to estimate the debiased main belt size distribution down to a few km in diameter (*10*). The problem for the NEA orbital distribution, however, is resolution; the limited number of Spacewatch NEAs do not provide enough coverage to normalize a wide-ranging probability distribution without leaving large tracts of (a, e, i, H) space without a single NEA (our B_{NEA} uses ~30,000 bins). Until the NEA inventory gains more entries, B_{NEA} cannot be directly used to produce statistically meaningful NEA population estimates.
31. Spacewatch has discovered and accidentally rediscovered 167 NEAs with 0.5 AU $< a <$ 2.8 AU, $e < 0.8$, $i < 35°$, and $13 < H < 22$. These asteroids have been winnowed from a larger set with a Spacewatch NEA probability calculation (*10*). 138 of these asteroids were detected within 50° of opposition. We determined that their (a, e, i) values are statistically similar to objects found within 20° of opposition, the region where B_{NEA} is most applicable.
32. W. H. Press, S. A. Teukolsky, W. T. Vetterling, B. P. Flannery, *Numerical Recipes: The Art of Scientific Computing* (Cambridge Univ. Press, Cambridge, 1992); L. Lyons, *Statistics for Nuclear and Particle Physicists* (Cambridge University Press, Cambridge, 1986).
33. We use a Monte Carlo technique to determine the statistical errors associated with our best fit. First, we generate many sets of fake asteroids according to our best-fit $n(a, e, i, H)$ distribution. The number of fake asteroids in each set is 138 (*31*). Next, we calculate new α_{IS} and γ values for each set using our maximum likelihood fit technique. Finally, we calculate a distribution for α_{IS} and γ and determine confidence limits. Assuming our best estimate for a parameter is p, we calculate the limiting value of $p+$ and $p-$ so that 34% of the values lie within the range ($p-$, p) and 34% lie within the range (p, $p+$). In this way, 68% lie within the range ($p-$, $p+$), yielding 1σ errors.
34. As of April 2000, the known NEA population of $H <$ 15 NEAs is 53 (*5*). Observations by the NEAT program suggest that $H < 15$ NEAs are ~80% complete (*8*). Using these values, we get ~66 NEAs with $H < 15$. Comparable numbers can be obtained using a different method; by dividing the number of already-discovered NEAs by the ratio of the number of new discoveries to total detections (new plus redetections) in the past year, there may be as many as 73 ± 7 NEAs with $H < 15$ [A. W. Harris, *Div. Dynam. Astron.* **31**, 16 (2000)]. Splitting the difference, we assume that there are 70 $H < 15$ NEAs. Because there are 4 $H < 13$ NEAs, the number between $13 < H < 15$ is ~66. The uncertainty in this value contributes to our method's systematic error.
35. P. R. Weissman, M. F. A'Hearn, L. A. McFadden, H. Rickman, in *Asteroids II*, R. P. Binzel, T. Gehrels, M. S. Matthews, Eds. (Univ. of Arizona Press, Tucson, AZ, 1989), pp. 880–920; W. K. Hartmann, D. J. Tholen, D. P. Cruikshank, *Icarus* **69**, 33 (1987); B. Gladman, P. Michel, Ch. Froeschlé, *Icarus*, in press.
36. D. L. Rabinowitz *et al.*, *Nature* **363**, 704 (1993); D. L. Rabinowitz, *Icarus* **111**, 364 (1994); *Icarus* **130**, 287 (1997).
37. J. W. Dohnyani, *J. Geophys. Res.* **74**, 2531 (1969).
38. Asteroid families produced by catastrophic collisions have cumulative size distribution slopes in excess of 2.5 [P. Tanga, *Icarus* **141**, 65 (1999)].
39. The cumulative size distribution of craters larger than 20 to 30 km on Earth has a power law slope of 1.8 (*11*). Craters on the lunar maria between 3 and 100 km in diameter have a power law slope of 1.7, though some of the larger craters have been enlarged by collapse. Correcting for crater collapse increases the slope to 1.84 [E. M. Shoemaker, *Annu. Rev. Earth Planet.* **11**, 461 (1983)]. Craters on the young Martian plains with diameters between 10 and 50 km have a power law slope of 2.0 [R. G. Strom, S. K. Croft, N. G. Barlow, in *Mars*, H. H. Kieffer, B. M. Jakosky, C. W. Snyder, M. S. Matthews, Eds. (Univ. of Arizona Press, Tucson, AZ, 1992), pp. 383–423)]. Craters on Venus with diameters larger than 35 km have a power law slope of ~2.0 [G. G. Schaber *et al.*, *J. Geophys. Res.* **97**, 13256 (1992).]

40. We thank J. Burns, L. Dones, A. Harris, T. Metcalfe, P. Michel, J. Plassman, T. Spahr, and G. Wetherill for valuable discussions and input to this study and two anonymous referees for their careful and constructive reviews. We gratefully acknowledge the computational resources provided to us for this project by Cornell University [both in the Department of Astronomy and at the Cornell Theory Center (CTC)], the University of Texas, the University of Arizona, the Osservatorio Astronomico di Torino, and the Observatoire de la Côte d'Azur. Finally, we thank C. Pelkie and the CTC for their help in making visualizations for this paper. Research funds were provided by grants from NASA's Planetary Geology and Geophysics program (NAGW-310), NASA's Near-Earth Object Observations program (NAG5-9082), and European Space Agency contract 14018/2000/F/TB. Travel support was provided by grants from NATO and NSF/CNRS. Spacewatch is funded by NASA, AFOSR, the Packard Foundation, and the Kirsch Foundation, as well as other organizations and individuals.

29 December 1999; accepted 12 April 2000